MOUNTAIN-PLAINS CONSORTIUM

MPC 18-368 | H. Mahmoud, M. Irfaee, and E. Hassan

Seismic Behavior of Steel Bridges with Fatigue-Prone Details

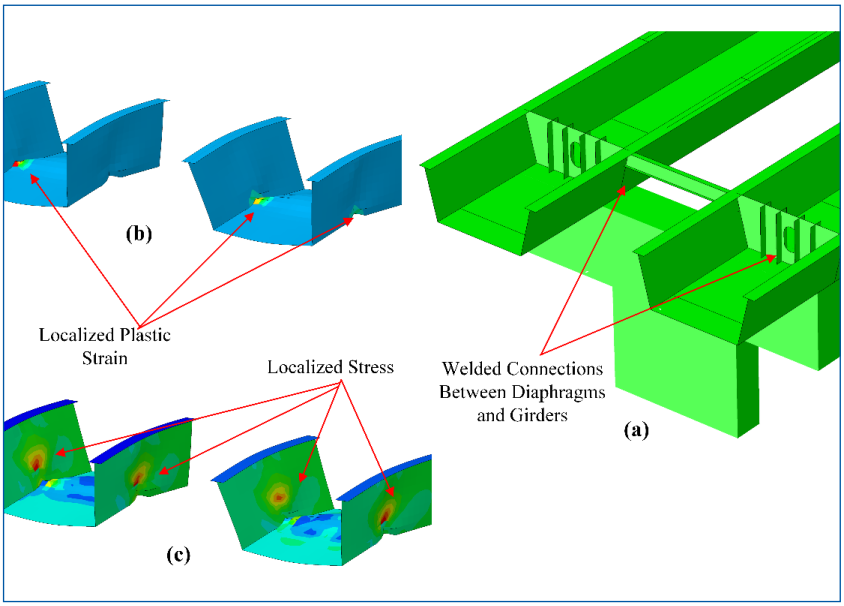

MOUNTAIN-PLAINS CONSORTIUM REGION 8

A University Transportation Center sponsored by the U.S. Department of Transportation serving the Mountain-Plains Region. Consortium members:

Colorado State University
North Dakota State University
South Dakota State University
University of Colorado Denver
University of Denver
University of Utah
Utah State University
University of Wyoming

Seismic Behavior of Steel Bridges with Fatigue-Prone Details

Hussam Mahmoud

Mazin Irfaee

Emad M. Hassan

Department of Civil and Environmental Engineering
Colorado State University
Fort Collins, Colorado

September 2018

Acknowledgements

The funds for this study were provided, in part, by the United States Department of Transportation to the Mountain-Plains Consortium (MPC). Matching funds were provided by Colorado State University. The data for this study were provided by Colorado State Patrol and Colorado Department of Transportation. Their assistance is greatly appreciated.

Disclaimer

ABSTRACT

Steel bridges with reinforced concrete substructures and steel superstructures are considered to have superior performance under earthquakes when compared with their reinforced concrete counterpart. Such performance reputation stems from the fact that few steel bridges have been subjected to strong ground motion in the last decade in North America. In addition to the lack of seismic exposure of bridges, research on the seismic performance of steel bridges' superstructure is limited to handful of studies. It is noteworthy that none of the previously conducted studies addressed the behavior of the bridge superstructure's fatigue details, which are designed for traffic loading, under earthquake loading. The studies also did not address the potential for the presence of existing cracks in bridges when an earthquake occurs. In the superstructure, fatigue is often the most prevalent problem in steel bridges and contributes to approximately 90% of existing cracks. The cracks are a result of the repeated traffic cycles exerted on the bridge, which is a primary concern in older bridges. In this study, the seismic behavior of a twin tub steel girder bridge is evaluated. Specifically, a detailed finite element model of the bridge in question is developed, and the model is subjected to a suite of ground motions. Of the two models developed, one did not include any initial cracks and one included a crack that presumably developed because of fatigue loading from usual traffic. The results of the analysis show large displacement of the bridge due to exposure to some of the earthquakes. In addition, the results show the potential for developing low cycle fatigue failure in some of the details, even in the absence of an initial crack. These results are critical as they highlight the importance for detailed assessment of the superstructure for bridges in moderate to high seismic regions.

TABLE OF CONTENTS

LIST OF FIGURES

1. INTRODUCTION

Steel bridges are vulnerable to earthquake ground motions, which have been highlighted during recent earthquakes in California and Japan (Astaneh et al. 1994; Bruneau 1996; and Itani et al. 2004). Failures at various steel bridge superstructure components were noted during these earthquake events. Component failure examples discussed by Itani et. al. (2004) included damage to bearings, end cross frames, web stiffeners, end cross frames and girders, and failure of shear connectors. Failure of these components highlighted the importance of establishing new design provisions that can allow for large cyclic deformations without loss of strength. It is important to emphasize that yielding in some of these components, at a specific earthquake intensity, is allowed as means for dissipating the seismic energy (Itani et al. 2004).

The vulnerability of steel bridges in general when subjected to ground motions has been highlighted by Itani et al. (2004). The study provided excellent examples of potential problems that could arise in steel bridges while drawing on recent events, such as the Petrolia, Northridge, and Kobe earthquakes. The study also discussed recent experimental and analytical investigations on steel plate girder bridges and their components under large demand. The results showed the importance of shear connectors for lateral force distribution to the end and intermediate cross frames, as well as the potential ductility that could be utilized in cross frames for dissipating seismic energy. Substantial insights were provided in the study on the performance of plate girder bridges under earthquake conditions.

While the concern over the seismic behavior of steel bridges is a valid one, a main question that remains to be answered is what the seismic behavior of a given bridge might be, particularly in relation to fatigue details where cracks might develop as a result of the large inelastic cycles during an earthquake. Furthermore, if a fatigue crack should develop under a typical service load, what is the likely behavior of the bridge in the presence of a fatigue crack? This is particularly an important question since many steel bridges have shown signs of excessive deterioration and fatigue cracking, particularly with bridges built before the mid-1970s. Fatigue cracks in steel bridges are considered a nuisance as they require periodic inspection and repair. Although the cracks are typically characterized by a stable propagation rate, the scatter in fatigue performance is difficult to quantify and could be on the order of thousands or even millions of cycles. If left unattended, the cracks could grow to reach critical length and threaten the integrity of the structure. While the issue of inspection and repair of bridges for fatigue cracks has attracted national and international concerns, the potential for concern could be easily elevated for older steel bridges showing signs of cracking in moderate to high seismic regions.

The overall goal of this study is to utilize detailed analysis techniques to understand the behavior of a twin tub steel girder bridge under earthquake loading in the presence or ~~d~~absence of fatigue cracking. The main goals in this study are to observe the effects of seismic activities on the performance of bridges and use low cyclic fatigue analysis to investigate the possibility of developing cracks due to seismic loadings.

2. LITERATURE REVIEW

2.1 Traditional Fracture Mechanics

Traditional fracture mechanics are based on the concept of the energy release rate, which is usually a function of a single parameter (e.g., stress intensity factor [K], J-integral, or Crack Tip Opening Displacement [CTOD]), and thus used as a one-parameter fracture criterion under specific conditions. The basic concept is that cracks in solids will propagate when the strain energy released by the crack extension exceeds the energy required for creating a new crack surface. By the difference in the assumption made regarding the yield zone surrounding the crack tip, traditional fracture mechanics can be categorized into linear elastic fracture mechanics (LEFM) with limited yield zone and elastic-plastic fracture mechanics with noticeable yield zone, as further discussed in the following sections. Some of the basic concepts are summarized from Anderson (1995). Based on the linear elastic assumption, the stress conditions around a crack tip can be determined, e.g., as an infinite plate with a crack length of 2a subjected to a far field axial stress σ normal to the crack. The stress intensity factor K_I for this mode can be determined by Equation 2.1 as follows:

$$K_I = \sigma\sqrt{\pi a} \ . \tag{2.1}$$

Since the LEFM assumption is invalid under large plastic behavior, several approaches with increased dominance zones have been developed, and are referred to as "Elastic-Plastic Fracture Mechanics." The most popular of which is the "J-integral" approach proposed by Rice (1968). The J-dominance zone is generally much larger than the K-dominance zone; hence, the J-integral approach is more applicable than LEFM in many situations involving large-scale yielding. CTOD was another approach widely explored even before Rice (1968) developed J-integral, mainly in the U.K., and later identified it to be analogous to the J-integral (Anderson, 1995).

In these approaches, the energy release rate serves as the main and only quantity to characterize resistance to fracture under different loading conditions, and thus the ability to absorb energy without fracturing has been introduced and named as "toughness." Under different constraint conditions, such as three-dimensional constraint, the resistance to fracture varies where the fracture toughness decreases under plane strain and increases under plane stress. According to common definitions, further fracture will occur when the energy release rate exceeds the toughness of the material. However, in reality, the stress state governs the potential for fracture. Consequently, a one-to-one correspondence between the energy release rate and toughness is acceptable for traditional fracture mechanics under specific constraint conditions. However, such an approach is invalid in the presence of excessive pre-crack plasticity, in which toughness actually depends on the size and geometry of the specimens and may significantly vary throughout a loading history.

Another issue regarding the use of traditional fracture mechanics, in cases with excessive yielding at the crack tip, is the validity of the singularity assumption, which is challenged by the presence of crack tip blunting, which is caused by large plasticization. The postulation of nonlinear elastic behavior in the J-integral leads to another issue. That is, when the crack grows, a plastic "wake" develops ahead of the crack as the crack moves forward. The wake area represents a region where the material has been plastically loaded and then elastically unloaded with residual plastic deformation, and hence the nonlinear elastic assumption violates such true material behavior.

If the plasticity remains confined to a relatively small region and the constraints are not low, the traditional fracture mechanic approaches are still the most popular and widely used because of their successful application in many practical situations over the years. However, if the plasticization grows

larger, or there exists a low level and more complex constraint conditions, the use of these traditional approaches is rather questionable.

Another issue regarding the use of traditional fracture mechanics approaches lies in their two-dimensional definition. It has been observed that thicker geometries are more prone to fracture, since there are larger constraints, and this effect cannot be considered by these approaches. Although there are approaches that attempt to add the additional stress constraints, such as the J-Q theory proposed by O'Dowd and Shih (1991), they are either difficult to apply or calibrate.

2.2 Traditional Fatigue

Fatigue failure can be defined as a series of fracture propagation when the material is subjected to cyclic loading. Depending on the number of cycles to failure, fatigue can be phenomenologically categorized as high-cycle fatigue and low-cycle fatigue. Repeated loadings are found to be very detrimental to materials with respect to stiffness and strength, even when the levels of stresses from the applied loads are far below the yield stress or ultimate strength.

The key question regarding fatigue strength is whether or not a crack will grow over a certain number of cycles. For some materials, when the cyclic stress range is below a certain value, the fatigue failure will not occur, and this value is usually called fatigue limit, endurance limit, or fatigue strength. However, for some other material, such threshold amplitude does not exist (Pyttel et al., 2011). In fracture mechanics, the limit is identified as the fatigue threshold ΔK_{th}, below which the fatigue crack will not grow farther (ΔK_{th} is the change in stress-intensity factor threshold). When the stress range amplitude near the crack tip, defined by the change in stress intensity factor ΔK, increases, the fatigue life decreases.

Currently, there are two types of modeling methodology considered for simulating the relation between fatigue life and stress range amplitude during cyclic loading. The first approach is based on fatigue crack propagation in terms of ΔK, and the other is based on cumulative fatigue damage as a function of the amplitude of stresses and strains. The cumulative fatigue approaches are mostly phenomenological, while the crack propagation theories are more dependent on physical mechanisms.

2.2.1 Crack Propagation

The basic concept for the crack propagation approach is that the crack growth increment at each cycle is calculated using a specific criterion, and once the crack grows to a critical length, the material is considered to have failed. The crack propagation rate is usually described as *da/dN*, where N is number of cycles, and such a rate is shown schematically in Figure 2.1, which comprises the three stages. Paris et al. (1961) first employed fracture mechanics to predict regions of stable fatigue crack growth under high-cycle fatigue (Stage II). Since then, the "Paris Law," which is Equation 2.2, has become the main approach for assessing crack growth under a low magnitude stress range.

$$\frac{da}{dN} = A(\Delta K)^n \tag{2.2}$$

where A and n are material constants.

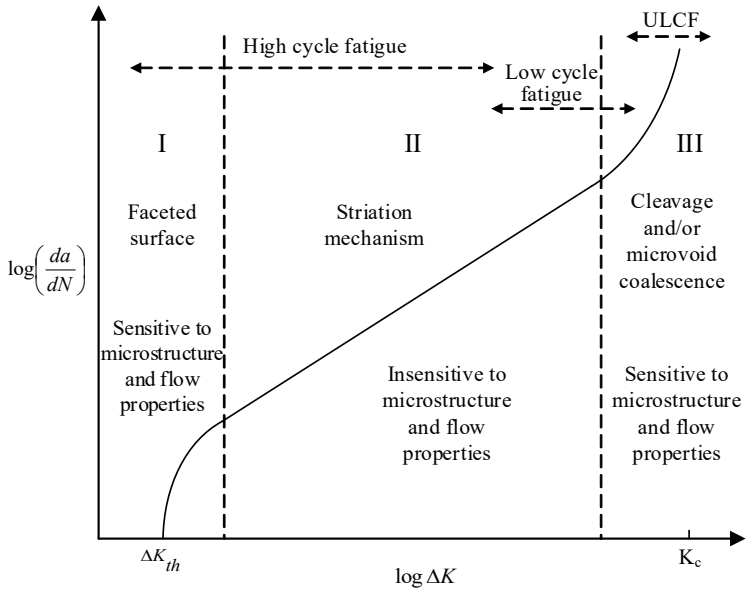

Figure 2.1 Stage and mechanisms of fatigue crack growth

In stage III, the crack growth rate indicates obvious acceleration, and the crack actually propagates in an unstable manner. In this stage, the fracture process, such as the microvoid coalescence and cleavage, also plays a role in crack extension. The overall crack growth is driven by the combined effects from fatigue and static fracture mechanisms. The contributions from fatigue decreases with increases in the maximum stress intensity factor K_{max}, and the failure mode gradually moves to complete monotonic fracture. Fracture under monotonic loadings, such as microvoid coalescence, cleavage, or both, is very sensitive to material properties, and hence such dependency is also high for stage III fatigue.

The main difference between fatigue failure and fracture under monotonic loadings lies in their different driving forces. In fatigue, a crack will grow in each eligible cycle with stress amplitude above the endurance limit. Meanwhile, under the same stress levels but without repeated loadings, fracture will not progress farther. Hence, the loading cycle is one of the additional driving forces for fatigue compared with monotonic fracture, and such extra driving force arises from the sharpening process of the crack tip in the reversed half cycles. At the same time, when the stress/strain fields during cyclic loadings are so large, even if the cyclicity halts, crack growth still occurs.

For traditional fatigue failure, stage III does not play an important role, since it takes a long time for a crack to grow from a small initial flaw to a critical size; in such cases, stage III probably only accounts for less than 1% of the total fatigue life. Studies on crack growth in region III are also scarce. For ULCF, stage III is the dominating phase, and typical fatigue theories do not apply. Under large loading demand, ULCF is the common failure mode; therefore, modeling of this fatigue stage should be explored.

2.2.2 Cumulative Fatigue Damage Approach

Fatigue damage develops with applied load cycles in an accumulative manner, and thus the cumulative fatigue damage theory has been the traditional approach for fatigue life assessment. The most common approach is the “linear damage rule” (LDR), which assumes fatigue damage accumulates in a linear way, and is also known as Miner’s rule (Miner, 1957), expressed as

$$D = \sum_i \frac{n_i}{N_i} \tag{2.3}$$

where n_i and N_i are the number of cycles and fatigue life, respectively, for the i th strain/stress range amplitude. Although many nonlinear rules have been developed to address the shortcomings of LDR through more extensive considerations of the stress/strain amplitudes, such as load sequence and deformation history effects, LDR remains the simplest and most frequently used cumulative rule. Fatigue damage is fundamentally the result of microstructural changes in the materials. Such changes on the microstructural level are assumed to have inherent relationships with macroscopic quantities, such as the stress (S-N curve) and strain (Manson-Coffin model) (Manson, 1965, and Coffin, 1954). By employing different macroscopic quantities, various criteria have been derived in order to describe the cumulative fatigue damage evolution in the framework of LDR. The commonly used quantities, stress and strain, are briefly introduced in some representative models in the following sections. A comprehensive review on the use of other quantities, such as energy and continuum damage mechanics-based approaches, can be found in Fatemi and Yang (1998).

2.3 Manson-Coffin Criterion for Low Cycle Fatigue

Studies on fracture predictions of stage III fatigue are relatively scarce. Fatigue at this stage is always featured with large plastic strain reversal, and thus the traditional stress-based fatigue approaches are not applicable to this stage. The number of cycles up to failure is usually less than 10 to 15 cycles since local strains are so large. In such cases, crack propagation is more prone to fracture rather than fatigue. Traditional low-cycle fatigue criteria, such as the strain-based approaches, only account for the fatigue part, and inevitably will gradually lose accuracy with the reduction in fatigue life (i.e., when fatigue life is expected to be below 10 cycles, which falls under the category of ULCF). As shown in Figure 2.2, as the plastic range $\Delta\varepsilon_p$ decreases, predictions by the Manson-Coffin criterion gradually start to overestimate the fatigue life, and the fracture also transfers from the surface fracture mode (fatigue) to the internal fracture mode (ductile fracture). In Figure 2.3, the damage, D_{Miner}, at the final fracture calculated by Miner's rule and the Manson-Coffin criterion is plotted; it gradually moves away from the supposed critical damage value "1" as the strain range increases. For predicting LCF life, however, the Manson-Coffin criterion coupled with Miner's rule have been proven sufficient.

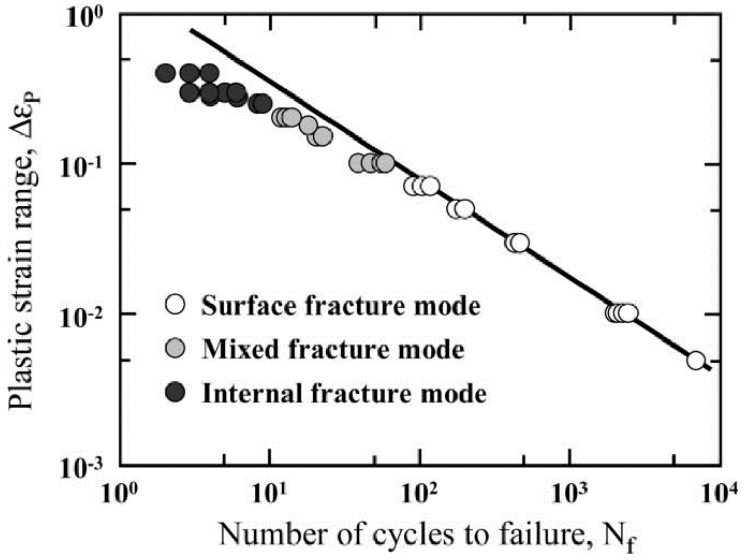

Figure 2.2 Fatigue life predictions versus real fatigue life (Kuroda, 2002)

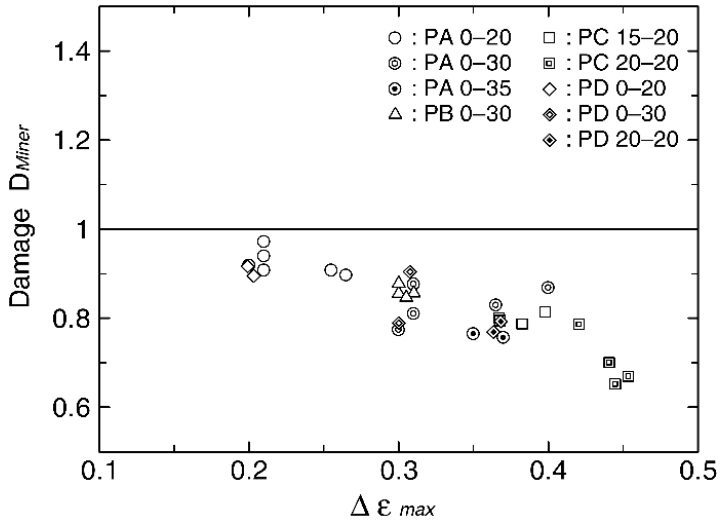

Figure 2.3 Relationship between the accumulated damage, D_{Miner}, and the maximum strain range $\Delta\varepsilon_{max}$ (Data from Tateishi et al., 2007)

3. NUMERICAL MODEL

3.1 Bridge Topology

To obtain realistic results, an actual bridge is used in the study. The bridge is a steel twin tub girder located on W 44th Avenue, crossing Interstate 25 in Denver, CO. Built in 1988, as shown in Figure 3.1, the bridge is 347 ft. long and 47 ft. wide. It is a continuous system, composed of three spans as shown in Figure 3.2 (a). Figure 3.2 (b) shows detailed geometry of the girder, including the web and flange thicknesses, while Figure 3.2 (c) shows a cross section of the bridge geometry illustrating the concrete slab thickness and the steel girder locations. The objectives of this study are to evaluate the effect of seismic activities at piers and abutment connections, assess the probability of devolving cracks at fatigue details, and determine local stresses and the potential for fracture at crack tip. Therefore, two models are developed: one without crack and one with crack at the mid-span. The bridge geometry is shown in Figure 3.3 (a). Figure 3.3 (b) shows a zoomed-in view of the deck and girders.

Figure 3.1 Pictures of the bridge used in this case study

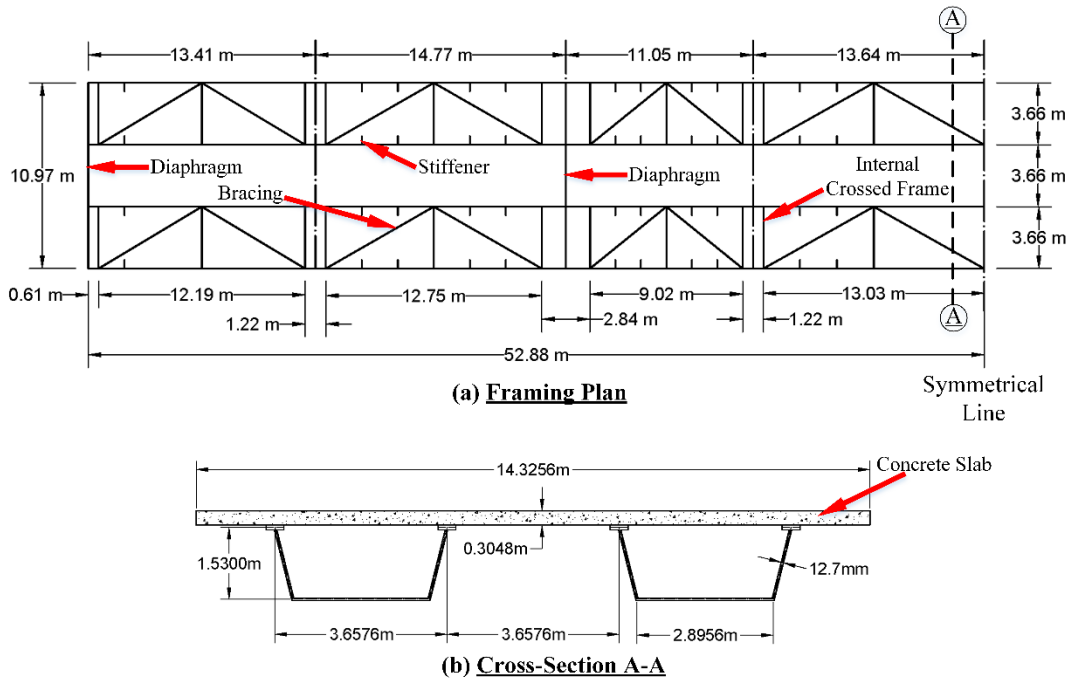

Figure 3.2 Details of the modeled bridge: (a) plan view, (b) girder elevation, and (c) cross sectional view

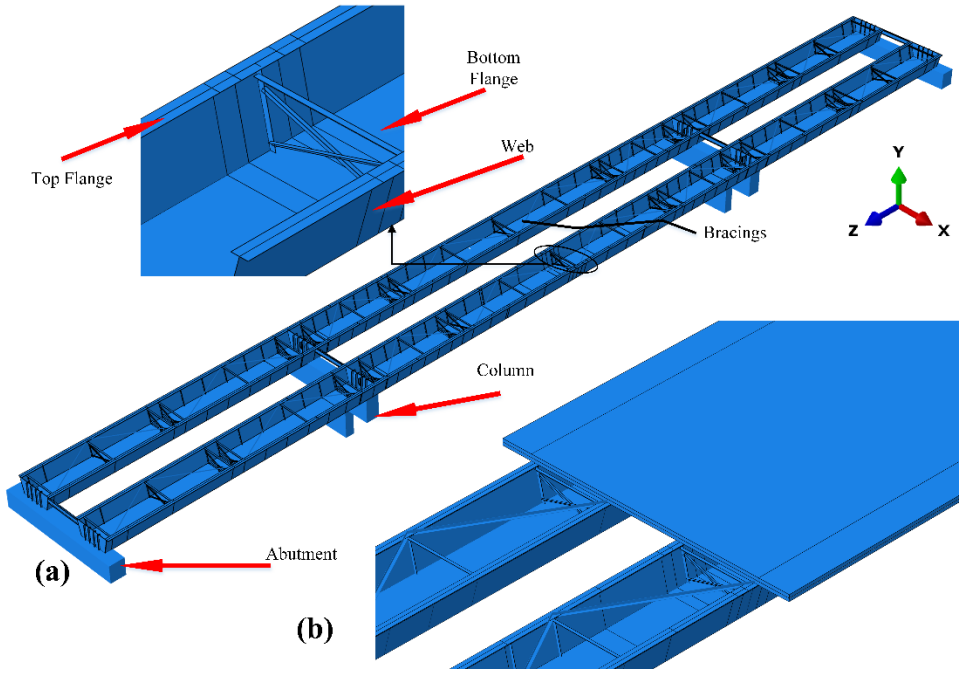

Figure 3.3 Bridge geometry: (a) entire bridge geometry, and (b) zoomed-in view of deck, girders, and bracings

3.2 Numerical Finite Element Modeling

3.2.1 Mesh Definition

Two types of the elements are utilized in the model, including three-node quadratic beams in plane (B22) line elements, and eight-node shell elements with reduced integration (S8R). The line elements are used to model the bracings, shear studs connecting the girders and concrete slab, and columns and abutments. The shell elements are used to model the main tub girders and their internal diaphragms as well as the concrete slab. The use of fine mesh allows for the localized stresses around the crack tip to be captured so that accurate estimates of the stresses and global response can be made. Since the value of the stresses and global response is sensitive to the mesh size, mesh refinements are specified around the crack tip. Figure 3.4 shows detailed mesh for the whole model, including the refined region.

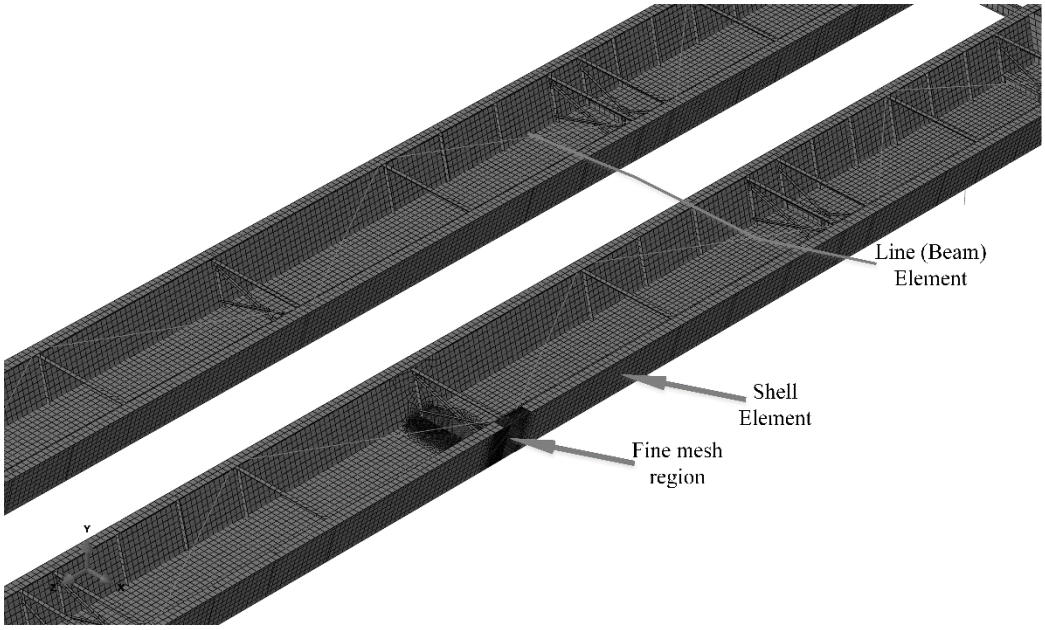

Figure 3.4 Finite element model of the bridge

3.2.2 Material Properties

Two types of materials are employed in the numerical finite element model, including steel and reinforced concrete. The steel used is A572 Grade 50 with yield stress of 50 ksi, ultimate strength of 65 ksi, elastic modules of 29,000 ksi, and Poisson's ratio of 0.3. The reinforced concrete is composed of concrete and reinforcing steel (also Grade 50) with an elastic modulus of 3,645 ksi, and a Poisson's ratio of 0.26. The reinforced concrete is modeled using shell elements with an impeded net of steel rebar. Rayleigh damping of 5% is considered based on the first, second, and third modes of vibrations.

3.2.3 Crack Definition

The crack is assigned at a transverse welded stiffener connection, which is part of an internal cross frame located along the bridge at its mid-length. Specifically, the crack is placed in one of the tub girders at the flange-to-web interface, as shown in Figure 3.5. The reason for selecting this region to introduce the crack is because this location represents the maximum positive bending moment. For the analysis case that included the cracks, the crack is assigned a length of 4 inches in the web and bottom flange. This initial

crack size represents a typical crack growth size that could be expected after two years of service if a crack was to initiate in this location. Specifically, the average daily traffic is assumed to be 500 cycles/day based on light daily traffic due to the bridge size and the location. The total number of cycles to propagate this crack size is calculated to be 365,000 cycles in two years using the Paris law for crack growth, which is the required inspection interval. Figure 3.5 shows the initial crack location and the directions in which each crack tip is assumed to have propagated.

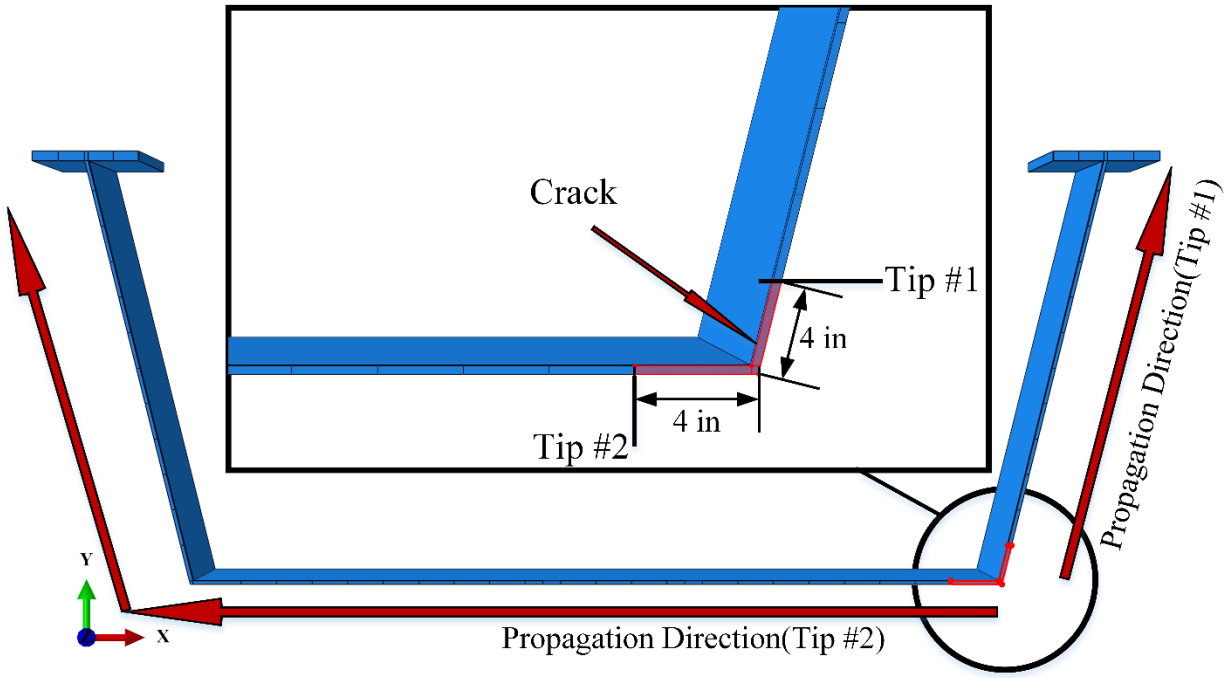

Figure 3.5 Initial location of the crack and the propagation directions

3.2.4 Applied Loads and Boundary Conditions

The loads assigned to the model are in the form of gravity loads, which is the self-weight of concrete and steel as per the 2012 AASHTO *Specification* (2012). No live loads or any kind of other loads were added to the model. The reason for ignoring the live load is because of the original assumption of light daily traffic. This is also in line with the recommendation in the AASHTO *Specification* (2012), in which it was noted that live loads should be calculated on a project-specific basis. The finite element models are subjected to a suite of ground motions as acceleration boundary conditions through the bottom ends of the columns/piers and abutments in the longitudinal direction of the bridge. The connections between the columns and the girders and between the abutments and the girders are simulated as fixed connections using couplings via ABAQUS. Figure 3.6 shows the boundary conditions and the applied loads as well as how the earthquake records are applied to the model.

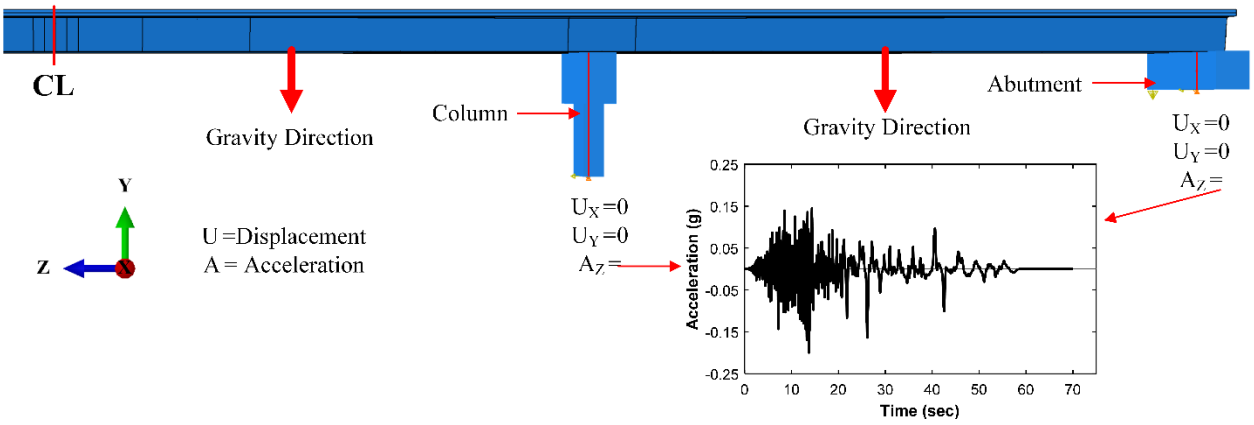

Figure 3.6 Model boundary conditions and applied loads

The suite of earthquake records, composed of seven different historical earthquakes, is selected in accordance with AASHTO (2011) *Guide Specifications*. Each earthquake has two perpendicular components in the horizontal direction, which presented a total of 14 records. These earthquake records are chosen with moment magnitude ranging from Mw 6.5 to 7.0, shear wave velocity ranging from 671 to 1,118 miles per hour, and a Joyner-Boore distance (Rjb) ranging from 12.4 to 18.6 miles. Denver, where the soil type is mostly a stiff soil, was chosen for the bridge location. Therefore, a stiff soil condition is considered in the earthquake records. Table 3.1 shows a summary of selected ground motions that include: record ID, which will be used in subsequent sections, magnitude, year, name and fault type of each earthquake as well as their recording stations, Rjb distance, and shear wave velocity.

Table 3.1 Earthquake characteristics

ID No.	Earthquake				Recording station	Rjb (Km)	Vs30 (mi/hr)
	Mag.	Year	Name	Fault Type			
1	6.6	1971	San Fernando	Thrust	LA - Hollywood Stor	24.5	1038
2	6.5	1979	Imperial Valley	Strike-slip	Calipatria Fire Station	14.4	675.1
3	6.5	1987	Superstition Hills	Strike-slip	Wildlife Liquef. Array	14.9	680.7
4	6.9	1980	Irpinia, Italy	Strike-slip	Mercato San. Severino	18.5	1148.2
5	6.9	1989	Loma Prieta	Strike-slip	Agnews State Hospital	15.1	786.5
6	6.7	1994	Northridge	Thrust	LA - Baldwin Hills	14.6	974.6
7	6.9	1995	Kobe, Japan	Strike-slip	Kakogawa	14.0	1023.6

The selected records are then scaled based on the bridge fundamental period in accordance with AASHTO *Guide Specifications* (2011), as noted in Wilson et al. (2015). To scale the earthquake motions, the mean of the ground motion response spectrums is developed and matched to the design response spectrum for the bridge location. As mentioned before, the soil type for the selected area is stiff soil. The USGS database and AASHTO *Guide Specifications* (2011) are used to develop the design response spectrum. Figure 3.7 shows the response spectrum for all the ground motion records before and after scaling.

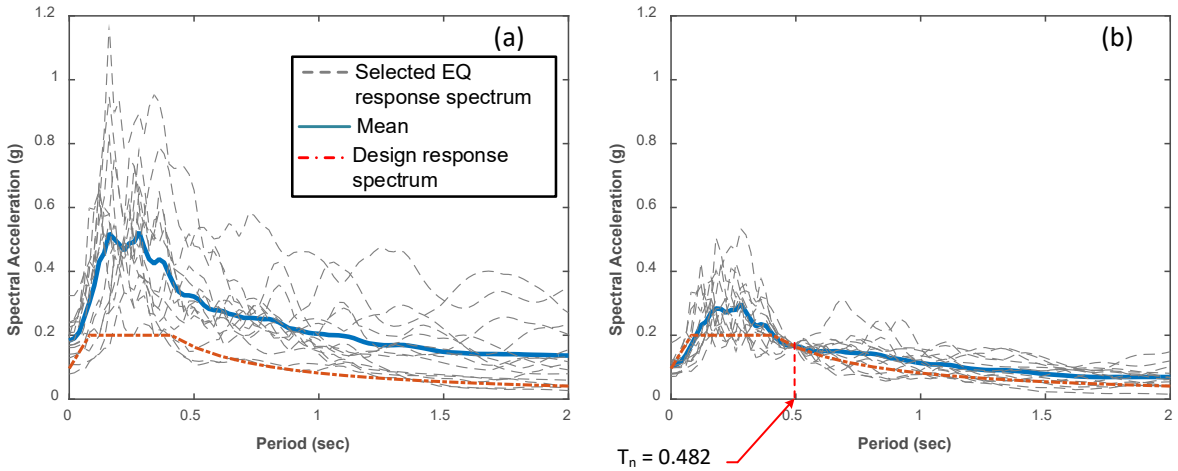

Figure 3.7 Response spectrum for selected earthquakes vs. AASHTO design response spectrum: a) before scaling and b) after scaling

4. RESULTS AND DISCUSSIONS

4.1 Fundamental Modes

The fundamental modes are analyzed by conducting an eigenvalue analysis. The bridge is modeled to have rigid connections at columns and abutments where the transitions and rotations are zero in all directions. Ten modes are gathered from the model, but only the first three are plotted below. Figure 4.1, Figure 4.2, and Figure 4.3 illustrate the modes for the bridge case study. The fundamental modes for the bridge show sine wave and twisting modes. The fundamental periods for each mode are 0.482 sec., 0.314 sec., and 0.24 sec., for mode 1, 2, and 3, respectively.

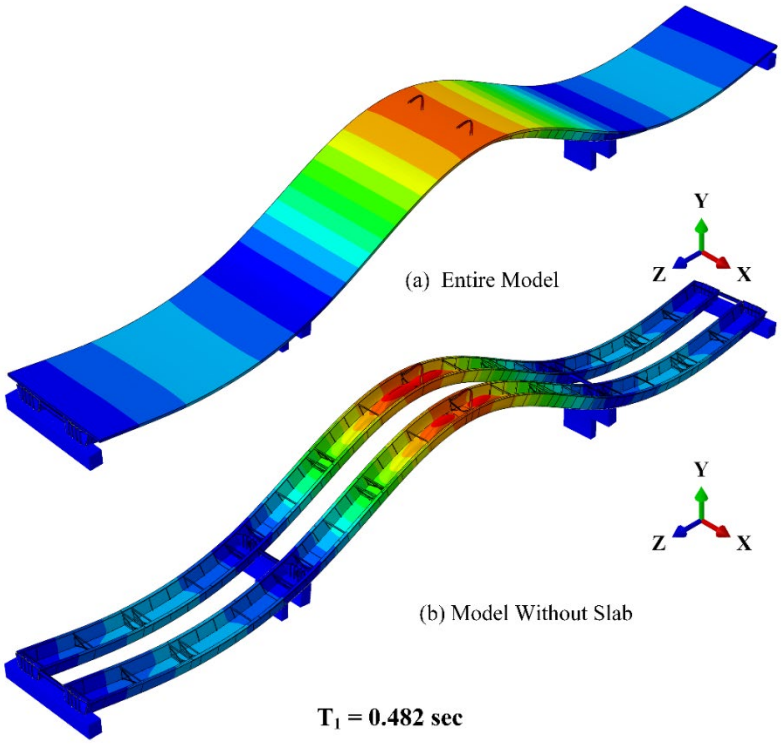

Figure 4.1 Shape of mode 1: a) entire model, and b) model without slab

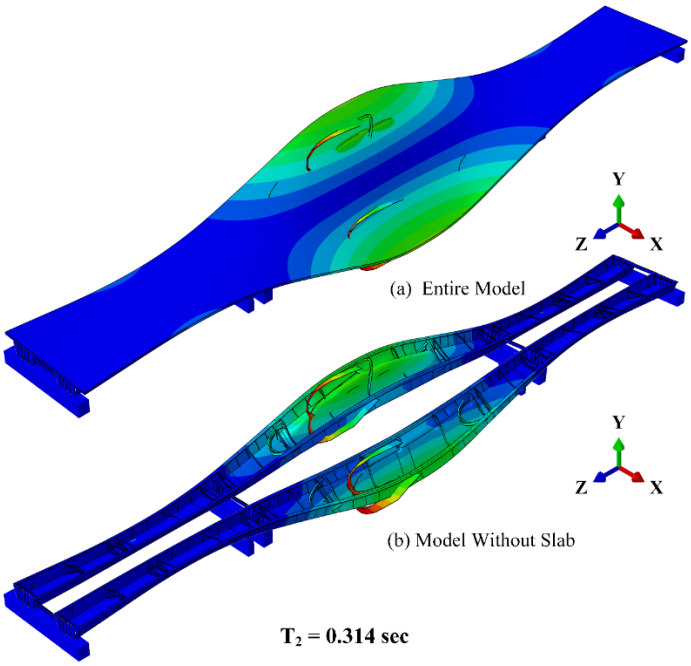

Figure 4.2 Shape of mode 2: a) entire model, and b) model without slab

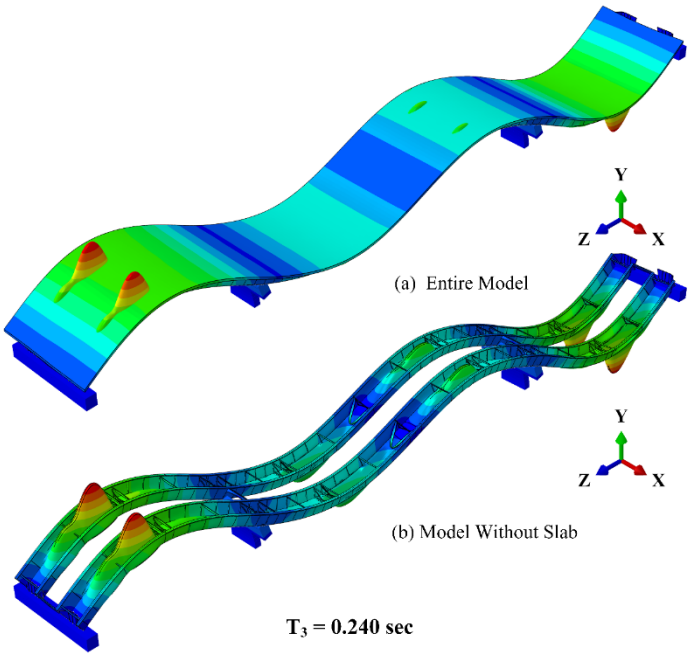

Figure 4.3 Shape of mode 3: a) entire model, and b) model without slab

4.2 Global Response from the Seismic Analysis

The maximum global deformation from all earthquakes ranged between 1 in. and 17 in. The maximum displacement was recorded to be along the Z-direction (which is the longitudinal direction) and is observed at mid-length of the bridge for all earthquakes. The largest displacement resulted from EQ#5, and is 16.96 in. The smallest displacement from all earthquakes used in this study is registered by EQ#14, which is -1.48 in. As expected, the bridge has a unique response to every earthquake that is a function of the intensity of the earthquake and its fundamental characteristics (frequency and duration). Figure 4.4 and Figure 4.5 show the global response for all earthquakes.

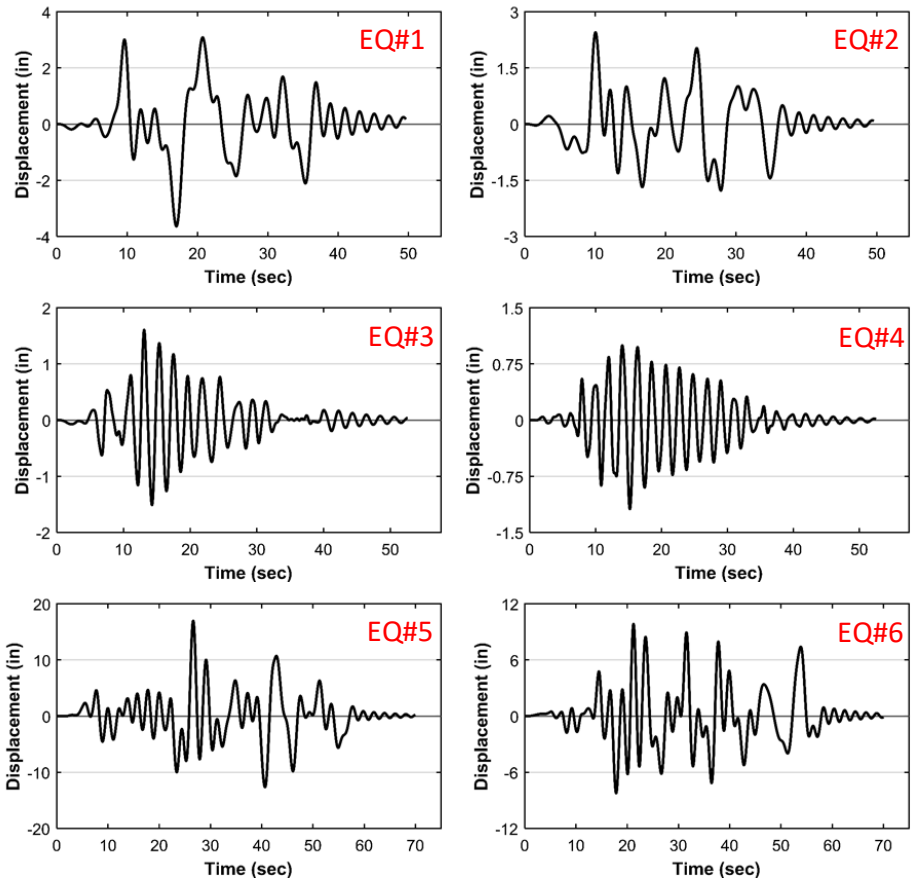

Figure 4.4 Global response from EQ#1 to EQ#6

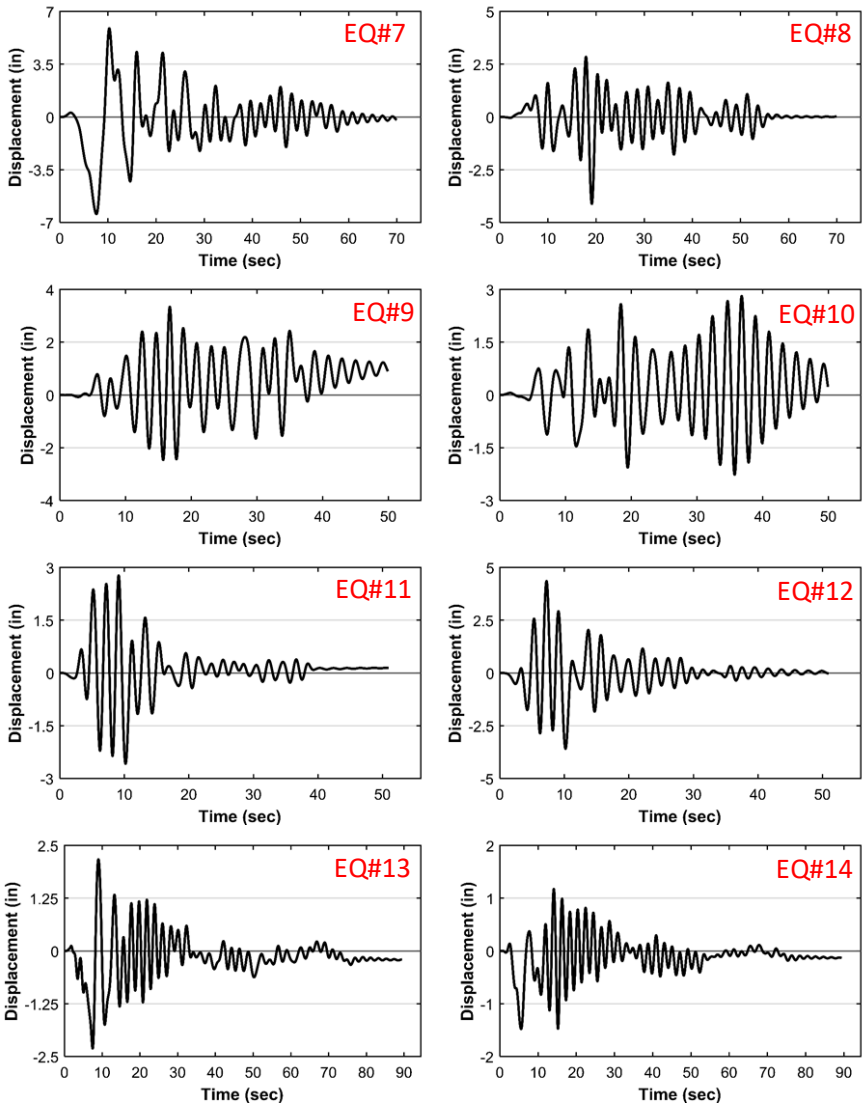

Figure 4.5 Global response from EQ#7 to EQ#14

4.3 Normal Stress at Piers

The largest normal stress values at the piers, resulting from all earthquakes, were collected and analyzed. More specifically, the presented values were obtained at the pier where the welded connection between the diaphragm and bottom flange is located adjacent to the intersection between web and flange. This welded connection represents one critical fatigue detail, which will be investigated later in detail. The maximum normal stress from all earthquakes ranged between 40 ksi and 60 ksi. EQ#5 and EQ#6 showed a very high stress cycle ranging between -55 ksi and 55 ksi. This cycle range continued to repeat between the times of 5 sec. to 55 sec. for both earthquakes. The remainder of the earthquakes also showed relatively high stress range values, although much less than those produced by EQ#5 and EQ#6. Figure 4.6 and Figure 4.7 show the normal stress versus time for all earthquakes.

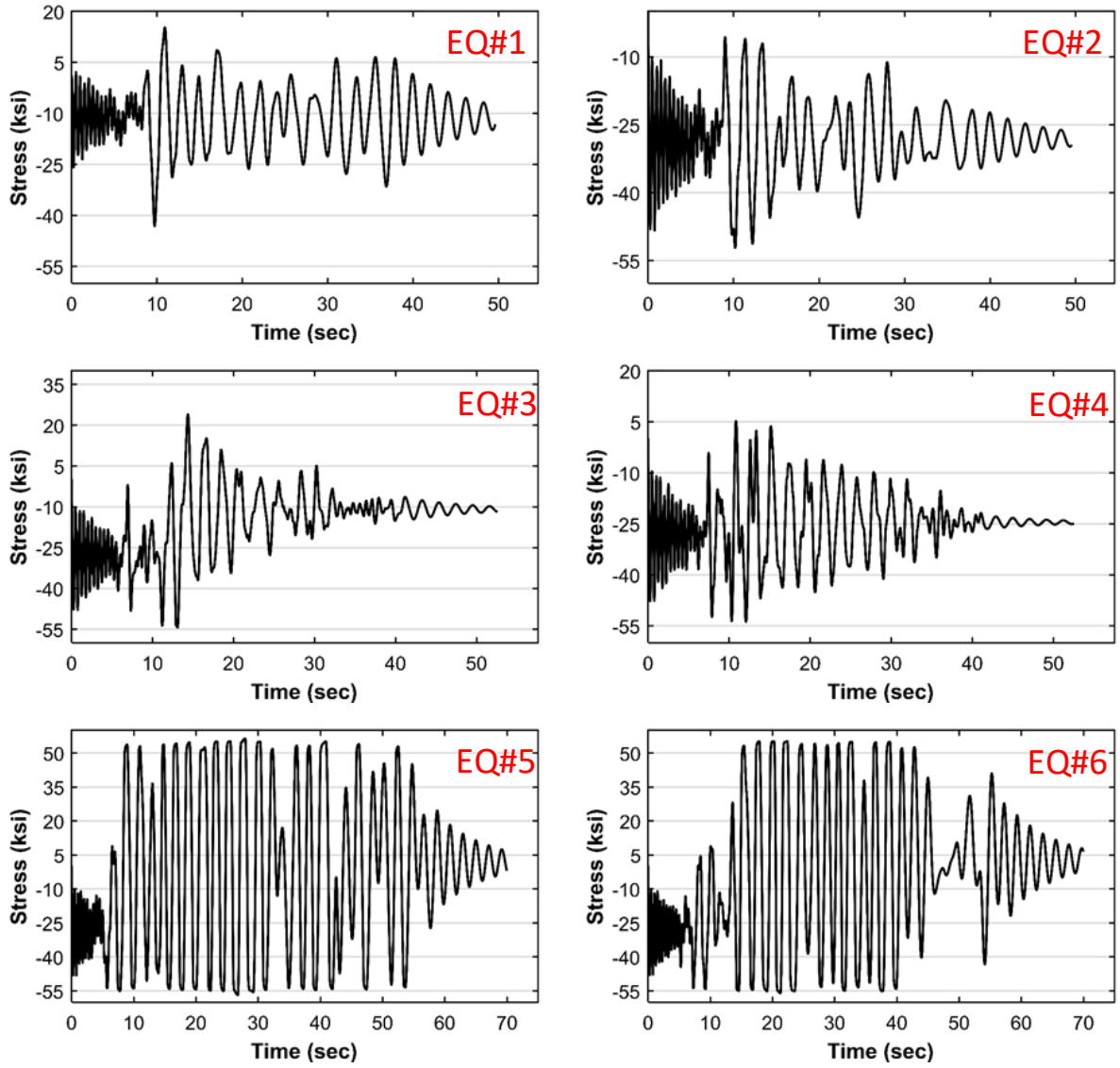

Figure 4.6 Normal stress at piers for earthquakes from EQ#1 to EQ#6

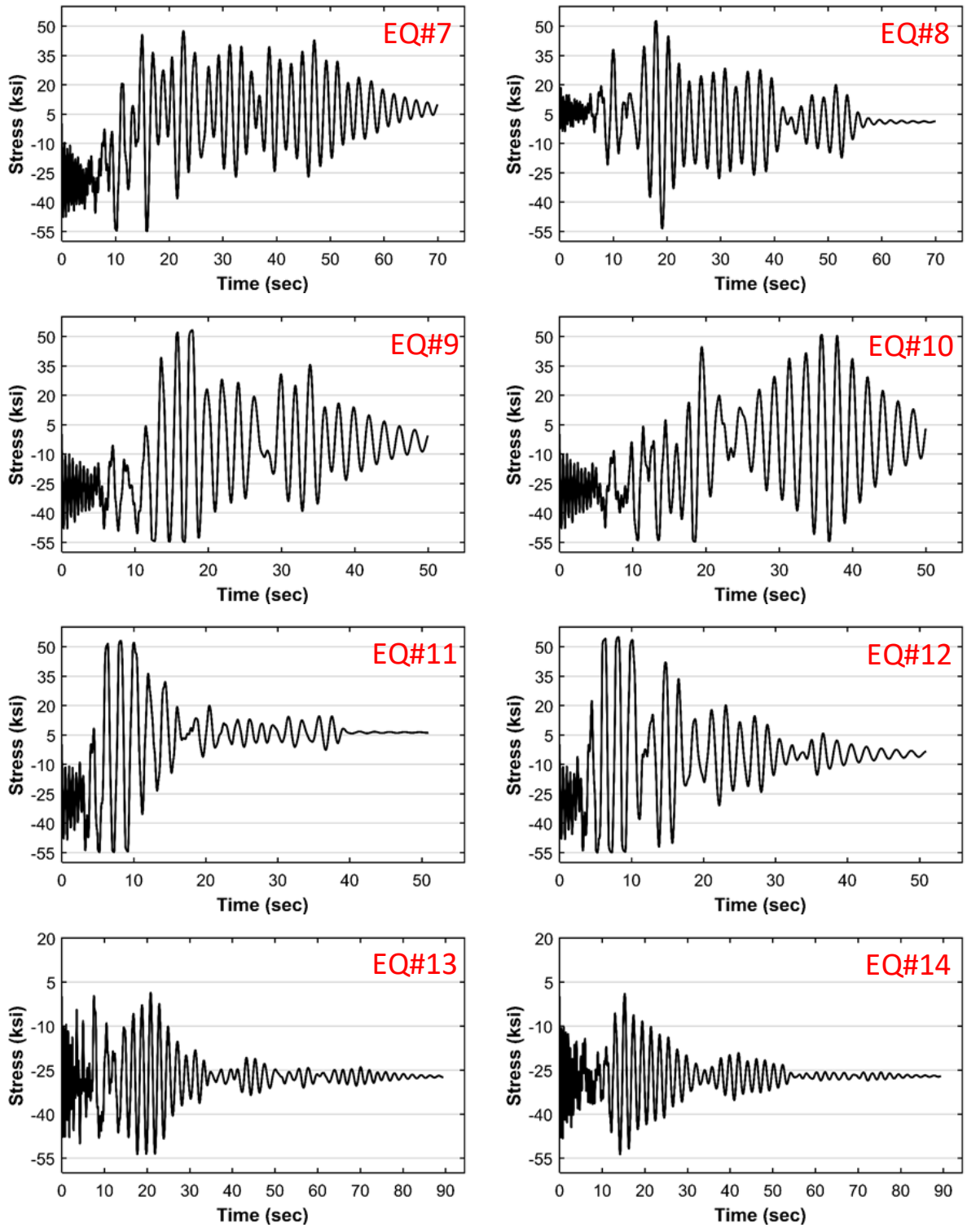

Figure 4.7 Normal stress at piers for earthquakes from EQ#7 to EQ#14

4.4 Exceeding Yielding Surface due to Seismic Loading

Figure 4.8 and Figure 4.9 represent when and how many times the seismic loading caused the stress distribution to exceed the yield surface limit with the corresponding displacement. These figures simply represent stress to be either zero or value. When stress has a value of zero, it means the behavior of bridge is linear elastic; when stress has a value larger than zero, it means the behavior is inelastic and the yield surface been reached. Most earthquakes showed a low number of times for exceeding the yield surface. As expected, the exceptions were EQ#5 and EQ#6, which showed very high numbers, corresponding to the large number of inelastic cycles. EQ#1, 13, and 14 showed a very low number of times for exceeding the yield surface, and EQ#2 showed fully elastic behavior.

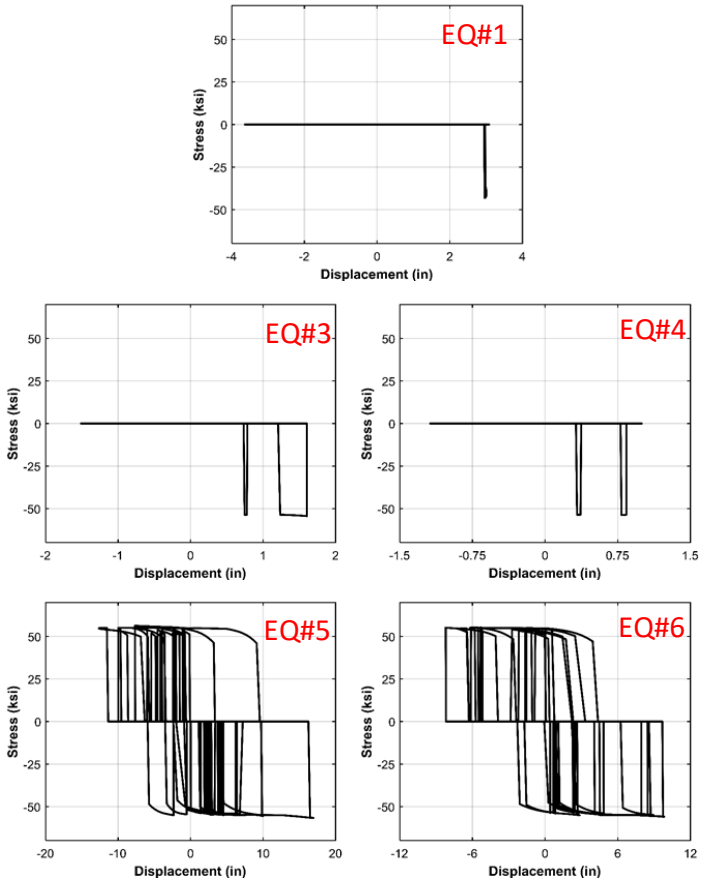

Figure 4.8 Exceeding yield stress surface vs. displacement for earthquake EQ#1 and earthquakes from EQ#3 to EQ#6

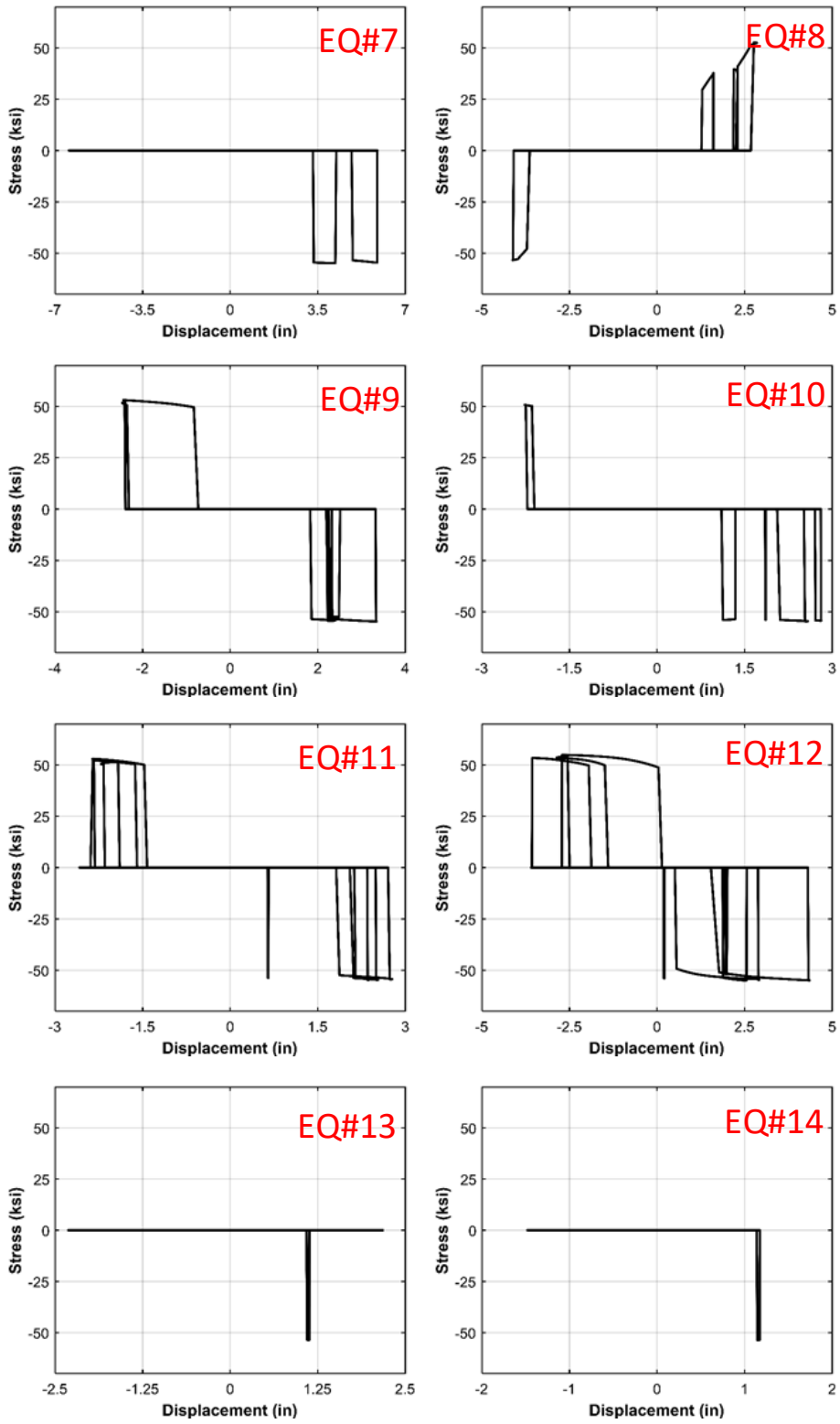

Figure 4.9 Exceeding yield stress surface vs. displacement for earthquakes from EQ#7 to EQ#14

4.5 Low Cycle Fatigue Analysis

The low cycle fatigue criterion used in estimating fatigue damage is the Coffin-Manson Model. This model describes the number of cycles, usually a small number, due to large repeated cycles of plastic strain. The relationship between the number of cycles and the plastic strain range by Coffin-Manson is as follows:

$$\frac{\Delta\varepsilon_{pl}}{2} = \varepsilon'_f(2N_f)^c \quad (4.1)$$

Where $\Delta\varepsilon_{pl}/2$ is the plastic strain amplitude, N_f is the total number of cycles to failure, ε_f' is the ductility coefficient, and c is the ductility exponent. Ductility coefficient (ε_f') corresponds to fracture strain, and the ductility exponent (c) ranges between -0.5 and -0.7 for most metal, with the most representative of -0.6 (Huang & Mahin, 2008). The values used for this case study are 0.2 and -0.6 for ductility coefficient (ε_f') and ductility exponent (c), respectively.

The location that showed sign of plastic strain in the model is at the welded connection between diaphragms and girders at the piers as shown in the Figure 4.10. This connection represents a fatigue detail with category C per the 2012 AASHTO *Specifications* (AASHTO, 2012). All low cycle fatigue analysis is performed on this connection using plastic strain data obtained at the bottom flange adjacent to the web. These time-history data were also re-analyzed to determine the number of cycles imposed on the detail. The number of cycles the detail is subjected to is then compared with the number of cycles calculated using the Coffin-Manson equation to determine if low cycle fatigue crack initiation is an issue. The results calculated show the connection to be at low cycle fatigue risk, therefore not at risk when subjected to EQ#5 and EQ#6. The remaining fatigue life for the earthquakes that showed no risk of failure (i.e., all earthquakes except EQ#5 and EQ#6) is around 99%. EQ#5 and EQ#6 reached the failure limit after the first five and eight cycles, respectively. It is worth noting that the total number of cycles from EQ#5 and EQ#6 was 34 and 25, respectively, which was calculated using rainflow analysis. The total number of cycles to failure was low, because the plastic strain range resulting from the earthquakes was very high and close to the failure strain. Table 4.1 summarizes the results for all earthquakes.

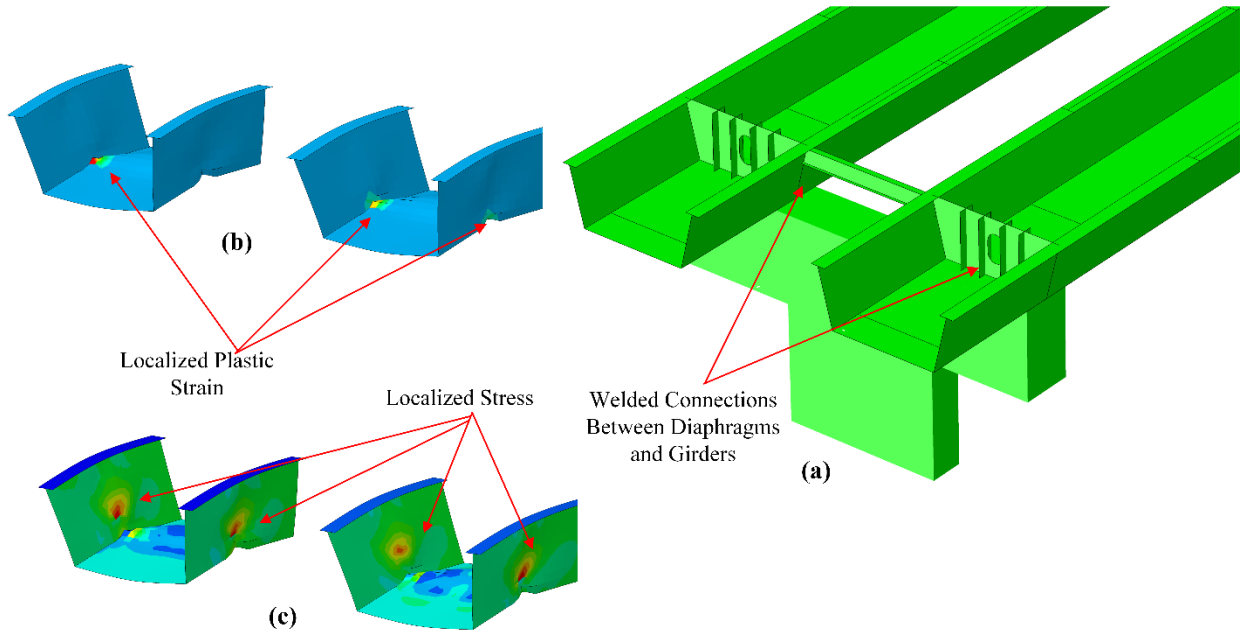

Figure 4.10 Welded connection between diaphragms and girders: a) the connection, b) localized plastic strain at the connection, and c) localized stress at the connection

Table 4.1 Low cycle fatigue results for both Coffin-Manson equation and rain-flow

Earthquake	Plastic Strain Range ($\Delta\varepsilon_{pl}$)	Number of cycles due to earthquake	Number of cycles to failure (N_f)	Remaining Number of cycles	Remaining Number of cycles %
EQ#1	0.00036965	1	56,938	56,937	99.99
EQ#2	0	0	infinite	infinite	infinite
EQ#3	0.00073214	2	18,262	18,260	99.98
EQ#4	0.00016124	2	227,873	227,871	99.99
EQ#5	0.1069	34	5	Failure	Failure
EQ#6	0.0778	25	8	Failure	Failure
EQ#7	0.0015	2	5,524	5,522	99.96
EQ#8	0.0017	4	4,484	4,480	99.91
EQ#9	0.0048	6	795	789	99.24
EQ#10	0.0015	5	5,524	5,519	99.90
EQ#11	0.0054	7	653	646	98.92
EQ#12	0.0148	8	122	114	93.42
EQ#13	0.000051187	1	1,537,990	1,537,989	99.99
EQ#14	0.000057281	1	1,274,908	1,274,907	99.99

4.6 Fatigue Evaluation in the Presence of a Crack

Because the analysis in the absence of a crack using EQ#5 represents the worst case, the same earthquake is used to evaluate the bridge response in the presence of a crack. Figure 4.11 (a) shows the crack location, and Figure 4.11 (b) shows a zoomed-in view of the crack. The results observed from the model with a crack are very similar to the model without a crack; although in the model with a crack, local concentration of plastic strain around the crack tips is observed, and consequently there is a high stress concentration around the crack tips, which is approximately 75.57 ksi. Figure 4.11 (c) shows local concentration of plastic strain around the crack tips where Figure 4.11 (d) shows local concentration of stress. Even though the developed plastic strain around the crack was small in comparison to the failure strain, the local stress was very high which exceeded the failure stress. The maximum displacement for the model with a crack was 14.96, which was less than what developed in the model with a crack. The presence of a crack provided slight flexibility to the model, resulting in lowering the response by approximately 1%. Figure 4.12 shows the global response for the model with a crack, while Figure 4.13 presents the local stress at the crack tip.

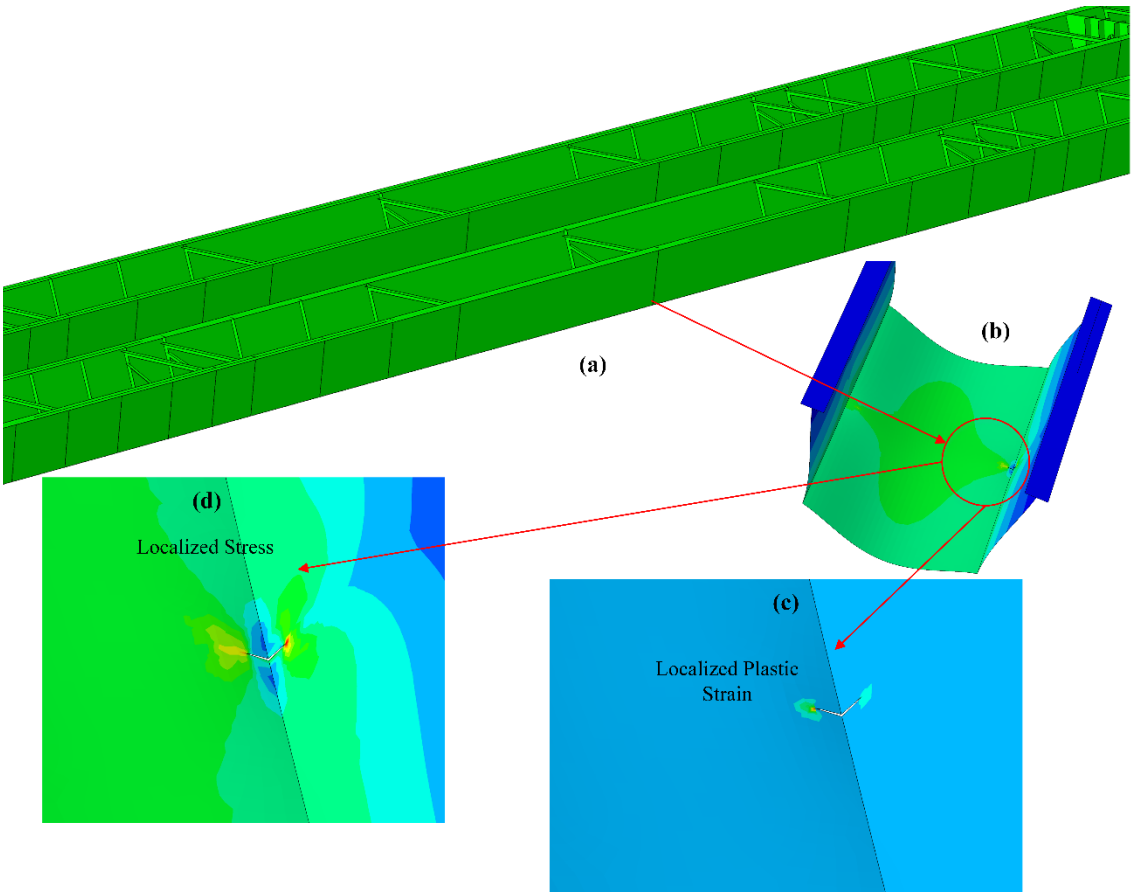

Figure 4.11 The crack location: a) crack location at the girder, b) zoomed-in view of the crack, c) localized plastic strain at crack tips, and d) localized stress at crack tips

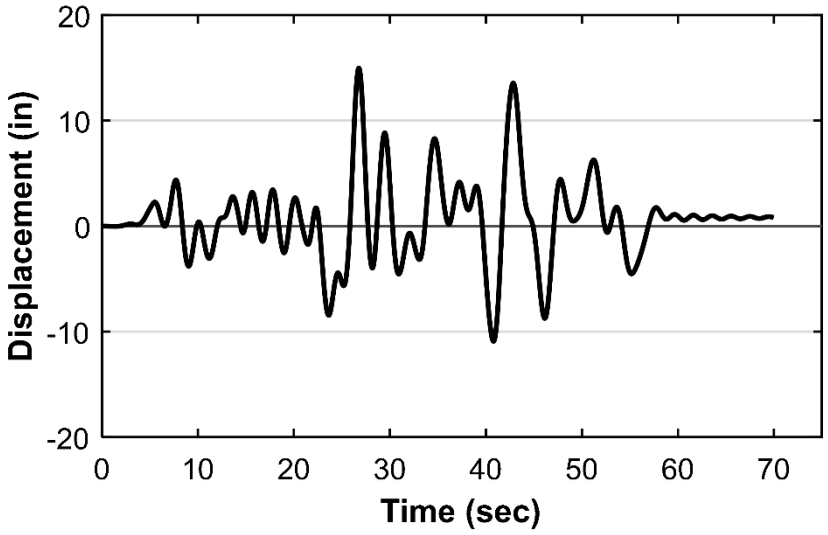

Figure 4.12 The global response for the model in presence of a crack

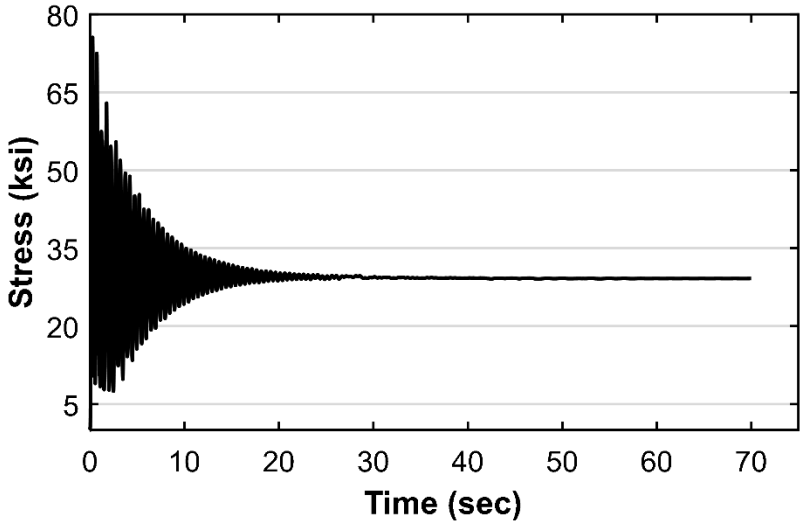

Figure 4.13 Local stress distribution at crack tip

5. SUMMARY AND CONCLUSIONS

In this study, detailed finite elements models of a twin-tub girder bridge with fatigue-prone detail were developed. The bridge was assumed to be located in Denver, CO, and subjected to light daily traffic. The model was then utilized to evaluate the low cycle fatigue behavior of the bridge when subjected to a suite of ground motions in the presence and absence of a fatigue crack. The Coffin-Manson approach was utilized to evaluate the low cycle fatigue behavior and calculate the total number of cycles to reach failure. The calculated number of cycles to failure was then compared with the total number of cycles, determined by rainflow counting analysis, the bridge was subjected to during a given earthquake. The following conclusions can be drawn:

Model without a crack

- The global displacement in the bridge, from all earthquakes, ranged between 1 in. and 17 in.
- Normal stresses at piers from all earthquakes ranged between 40 ksi and 60 ksi.
- EQ#5 and EQ#6 resulted in the maximum demand on the bridge as manifested by high stress ranges.
- Seismic loadings caused low cycle fatigue failure in the bridge.

Model with crack

- Local plastic strain around the crack tip was very minimal, suggesting relief in strain in the presence of a crack.
- The presence of a crack resulted in more flexibility in the bridge model, which caused minor reduction in global displacement of about 1%.
- The model with a crack showed small values of plastic strain and very high values of stress around the crack tips.

6. REFERENCES

AASHTO (2012). *AASHTO LRFD Bridge Design Specifications*. 8th ed. Washington. DC.

AASHTO (2011). AASHTO Guide Specifications for LRFD Seismic Bridge Design. 2nd ed. Washington. DC.

Anderson, T. L. 2005. Fracture mechanics: fundamentals and applications. Boca Raton, FL: CRC press.

Ahmad M. Itani, Michel Bruneau, Lyle Carden, and Ian G. Buckle. (2004). "Seismic Behavior of Steel Girder Bridge Superstructures." *Journal of Bridge Engineering*, Vol. 9, No. 3.

Astaneh-Asl, A., Bolt, B., McMullin, K. M., Donikian, R. R., Modjtahedi, D., and Cho, S., (1994). Seismic performance of steel bridges during the 1994 Northridge Earthquake. Rep. No. UCB/CE-STEEL-94/01, Dept. of Civil Engineering, Univ. of California at Berkeley, California.

Bruneau, M., Wilson, J. W., and Tremblay, R. (1996). "Performance of steel bridges during the 1995 Hyogoken-Nambu (Kobe, Japan) earthquake." *Can. J. Civ. Eng*., Vol. 23, No. 3, 678–713.

Coffin, L. (1954). "The problem of thermal stress fatigue in austenitic steels at elevated temperatures." In Symposium on Effect of Cyclic Heating and Stressing on Metals at Elevated Temperatures. ASTM International.

Fatemi, A., and Yang, L. (1998). "Cumulative fatigue damage and life prediction theories: a survey of the state of the art for homogeneous materials." *International Journal of Fatigue*, 20(1), 9-34.

Huang, Y., & Mahin, S. A. (2008, June). "A cyclic damaged plasticity model: Implementation and applications." In 10th International LS-DYNA User's Conference.

Manson, S. S. (1965). "Fatigue: a complex subject—some simple approximations." *Experimental Mechanics*, 5(7), 193-226.

O'Dowd, N. P. and Shih, C. F. (1993). Two-parameter fracture mechanics theory and applications. NUREGjCR5958, CDNSWSjSME-CR-16-92, Brown University.

Paris, P. C., Gomez, M. P., and Anderson, W. E. (1961). "A rational analytic theory of fatigue." *The Trend in Engineering*, 13(1), 9-14.

Pyttel, B., Schwerdt, D., and Berger, C. (2011). "Very high cycle fatigue–is there a fatigue limit?" *International Journal of Fatigue*, 33(1), 49-58.

Rice, J. R. (1968). "A Path Independent Integral and the Approximate Analysis of Strain Concentration for Notches and Cracks." *Journal of Applied Mechanics*, 35, 379-386.

Wilson, T., Mahmoud, H., and Chen, S. (2015). "Seismic performance of skewed and curved reinforced concrete bridges in mountainous states." *Engineering Structures*, Vol. 70, 158-167.